Journal of Applied Physics

Computational predictions of stable phase for antiperovskite Na_3OCl via tilting of Na_6O octahedra

Cite as: J. Appl. Phys. **124**, 164106 (2018); https://doi.org/10.1063/1.5047833
Submitted: 10 July 2018 . Accepted: 02 October 2018 . Published Online: 29 October 2018

Tan-Lien Pham, Abdus Samad, Hye Jung Kim, and Young-Han Shin

JOURNAL OF APPLIED PHYSICS **124**, 164106 (2018)

Computational predictions of stable phase for antiperovskite Na_3OCl via tilting of Na_6O octahedra

Tan-Lien Pham, Abdus Samad, Hye Jung Kim, and Young-Han Shin[a)]
Multiscale Materials Modeling Laboratory, Department of Physics, University of Ulsan, Ulsan 44610, Republic of Korea

(Received 10 July 2018; accepted 2 October 2018; published online 29 October 2018)

We study the structural stability of crystalline Na_3OCl in terms of cohesive energies and phonon spectra through the tilting of Na_6O octahedra. We prove that the crystal Na_3OCl can be stabilized through octahedral tilts by comparing 14 tilted structures that are consistent with the Howard and Stokes' group-theoretical analysis of the octahedral tilting in perovskites. We found that all the 14 tilted structures of Na_3OCl have lower energies than the cubic $Pm\bar{3}m$ structure by about 11 to 16 meV per five-atom unit cell. The tilt angles along the pseudocubic [100], [010], and [001] directions vary in the range of 2.6°–9.3°. While the Pnma and $P2_1/m$ structures of Na_3OCl are found as the two most stable ones, only the $P2_1/m$ phase has stable phonon vibrations with a direct band gap of 3.38 eV at the Γ point. *Published by AIP Publishing.* https://doi.org/10.1063/1.5047833

I. INTRODUCTION

Antiperovskite materials have attracted much attention due to their applicability in various technologies. Many researches have been performed to understand the ion transport, magnetism, and superconductivity of the antiperovskite materials.[1–5] These materials have interesting physical properties like giant magnetoresistance in Mn_3GaC[6] and the near-zero temperature coefficient of resistivity in Mn_3NiN.[2] Especially, alkali metal oxyhalides such as Li_3OCl, Li_3OBr, Na_3OCl, and Na_3OBr have demonstrated superionic conductivity.[7]

Since organic liquid electrolytes used as a Li transport medium in the traditional rechargeable batteries are flammable, they suffer from safety issues. During charge and discharge processes, the formation and growth of anode dendrites through the electrolyte to the cathode results in short-circuit and incendiary consequences. Present-day Li-ion batteries are fabricated in the discharged state to avoid any alkali metal in the anode. However, the anode of a high-voltage cell reacts with the organic-liquid electrolyte and forms a solid-electrolyte interphase (SEI) passivation layer. Recently, there has been growing interest in solid-state electrolytes as they can provide non-flammable, lower-maintenance batteries with a longer life cycle and a lower self-discharge.[8] The solid electrolytes have an energy gap large enough above the Fermi energies of metallic lithium and sodium to eliminate the formation of SEI layers. Solid electrolytes also have the potential to improve battery performance since they have the potential to be utilized with elemental metals such as lithium or sodium for the anode, which would increase the energy density of the battery. Therefore, all-solid-state batteries are emerging as suitable candidates for large-scale energy storage.

Na-ion batteries are considered as a possible lower-cost alternative to Li-ion batteries due to the abundance of sodium in the earth's crust.[9] Solid electrolytes have not yet been extensively employed in commercial batteries as they suffer from poor ionic conduction at acceptable temperatures and insufficient stability with respect to the anode. The discovery of solid glassy electrolytes evolved from an antiperovskite structure overcomes the disadvantages of traditional rechargeable batteries such as the formation of dendrite, the presence of SEI, large volumetrics[10] and results in a high ionic conductivity at room temperature in the order of 10^{-4} to 10^{-3} S cm^{-1} up to a stellar value of 0.025 S cm^{-1} and low activation energies in the range of 0.2–0.3 eV.[8] Therefore, Li/Na rich antiperovskites (Li/NaRAP) are promising in solid-state batteries.

Hippler studied the single crystal structure of Na_3OCl and observed that oxygen is surrounded by six Na atoms to make distorted octahedra and chlorine is coordinated by 12 Na atoms.[11] Zhao and Daeman and Zhang *et al*. reported that Li_3OCl had a cubic structure ($Pm\bar{3}m$),[12,13] and Zinenko and Zamkova showed the similar phonon spectra of Na_3OCl[14] and Chen *et al*. pointed out phonon instability at R and M points in the cubic structure.[15]

Antiperovskite (A_3XY) is similar to perovskite (ABX_3) with reversed cation (A,B) and anion (X,Y) positions. Most perovskites undergo symmetry-breaking transitions resulting from the distortions or rotations of the octahedra under temperature and pressure variations.[15] A method for describing and classifying tilted octahedra only in cell-doubling perovskite is shown by Glazer notation which uses symbols of the type $a^*b^*c^*$. The component tilts can be taken about the pseudocubic axes of the untilted perovskite. a, b, and c denote the magnitude of the angles of tilt about the three unit-cell axes in accordance to directions [100], [010], and [001], respectively. Equality of tilts is represented by repeating one of the letters, that is, *aac* means equal tilts along the [100] and [010] directions with a different tilt along the [001] direction. In addition to the magnitude of the tilt, it is also necessary to consider the sign of the tilt. If a particular octahedron is tilted about an axis, then the next octahedron

[a)]hoponpop@ulsan.ac.kr

along this axis can be tilted in the same or opposite directions (in-phase or out-of-phase). The superscript * being +, −, and 0 indicates in-phase, out-of-phase, and no tilt along a specific axis, respectively. Glazer showed 23 possible simple tilt systems corresponding to 15 space groups.[16] In Howard and Stokes group-theoretical analysis, 15 space groups are listed. Eight tilt systems missing have higher symmetry than the corresponding space group.[17] The knowledge of tilt octahedra is valid in studying the structural instability of perovskite and antiperovskite materials.

In our previous studies, we worked out a number of strategies to enhance the electrochemical performance of anode materials for rechargeable metal ion batteries. One of the main goals of these studies was to search efficient alternatives to Li ions where we concluded that cheap, abundant, and non-toxic Na was the most possible alternative for Li.[18–21] It is already mentioned that Li_3OCl is promising as a solid-state electrolyte. Being a structural analog of Li_3OCl, Na_3OCl can be the best choice as a solid electrolyte for Na ion batteries. However, similar to cubic Li_3OCl, cubic Na_3OCl also has negative frequencies at the M and R points in its phonon dispersions. Following the work of Chen *et al.*,[15] we were able to show that the energy of Na_3OCl can be lowered by the tilting of Na_6O octahedra and stable phonon modes can be achieved. Thus, in this study, we have found the two most energetically stable structures of Na_3OCl are Pnma and $P2_1/m$, but only monoclinic $P2_1/m$ phase is dynamically stable among the 14 tilted phases. As the other phases of Na_3OCl are unstable, we focus on studying the structure and properties of the $P2_1/m$ phase only. The Bader and Born effective charges of Na, Cl, and O show that monoclinic $P2_1/m$ is an ionic crystal. The cubic nontilted phase and the tilted $P2_1/m$ phase have a similar band gap of about 3.40 eV.

II. METHOD

All our calculations are based on density functional theory implemented in the Vienna *Ab Initio* Simulation Package (VASP).[22] The electron–electron exchange-correlation is performed using the generalized gradient approximation (GGA) proposed by Perdew-Burke-Ernzerhof.[23] The electron–ion interactions are described by the projector augmented wave (PAW) method.[24] Through the convergence examination of *k*-points and cutoff energies for the cubic and the tilted Na_3OCl, we use 700 eV for the cutoff energy and $6 \times 6 \times 6$ (cubic phase) and $8 \times 8 \times 8$ (tilted phases) for the *k*-point meshes. Structures are relaxed and optimized until the Hellmann–Feynman force on each atom is less than 0.001 eV/Å. The Birch-Murnaghan equation of state is used to fit the energy versus volume curve during the optimization process. The tetrahedron method with Blöchl corrections is chosen to obtain a very accurate total energy in full relaxation calculations of each structure.

Phonopy code[25] is used to generate the phonon dispersion curves and verify the space group of the 15 tilted structures before and after relaxation. The *k*-path in first Brillouin zone is selected using Xcrysden program.[26] Band structure and density of states calculation are obtained through the generalized gradient approximation (GGA) and hybrid functional Hyed-Scuseria-Erznerhof (HSE) methods.[27]

III. RESULTS AND DISCUSSION

Optimization and relaxation process gave the lattice parameter of Na_3OCl cubic primitive cell $a = 4.538$ Å using the GGA method and $a = 4.382$ Å using the local density approximation (LDA) method. In the experiment, Hippler reported $a = 4.496(2)$ Å.[11] Due to the approximation of the exchange-correlation energy functional, convergence of the used basis set, and how well the pseudopotentials compare to full potential all electron methods, our calculated results are not exactly the same as the experiment but it is being acceptable. In Kohn-Sham's equation, the exchange-correlation energy functional is computed approximately by LDA or GGA methods. LDA is generally not accurate enough to describe the energetics of chemical reactions (heats of reaction and activation energy barriers), leading to an overestimation of the binding energies of molecules and solids in particular.[28,29] GGA is presented to overcome such deficiencies. Therefore, the results obtained from GGA are much better than the LDA method. As compared to the experimental results, LDA result is underestimated by 2.54% while GGA result is overestimated by 0.93%.

At first glance in Fig. 1(a), we easily realize that the phonon dispersion curves show negative frequencies at the M and R points. It means that the lattice vibrations are unstable at M and R symmetry points of the cubic $Pm\bar{3}m$ Na_3OCl in a $3 \times 3 \times 3$ supercell. We already checked for phonon convergence from $1 \times 1 \times 1$ primitive cell to $6 \times 6 \times 6$ supercell, the results show that phonon modes in $3 \times 3 \times 3$ supercell have very similar properties to them in larger supercell size. The soft phonon modes occur at M and R which still remain negative when cell size increases but a phonon mode at M is slightly negative for the enlarged cell size. Phonon curves illustrate the elastic vibrations of atomic lattice points of crystal. When cell size increases, the interaction between lattice points becomes more practical and boundary effect is reduced which increases the computational

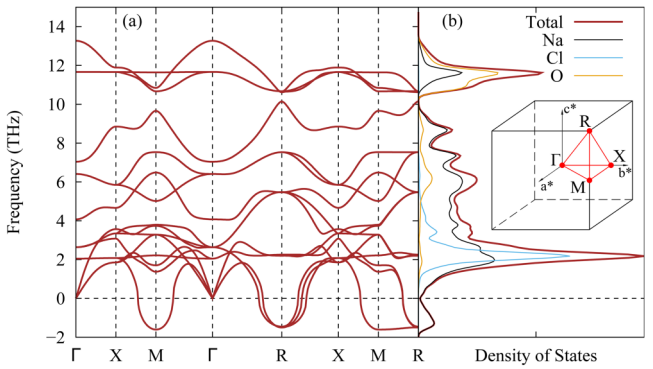

FIG. 1. (a) Phonon band structure and (b) density of states of the cubic $Pm\bar{3}m$ phase. The soft modes at M and R points in the phonon band structure indicate that the cubic $Pm\bar{3}m$ phase is dynamically unstable. The red curve in (b) represents the total phonon density of states. The black, blue and orange curves corresponds to the partial phonon density of states of Na, Cl, O, respectively. The *k*-path in the first Brillouin zone is shown in the inset. The unstable soft modes dominantly come from Na.

accuracy. In phonopy, the generation of force constants relies on the finite displacement method. Na_3OCl is a non-metallic crystal which is polarized due to atomic displacements. The macroscopic electric field is generated by the long-range character of the Coulomb forces that are associated with long wave longitudinal optical phonons.[30] Through non-analytic term correction, the LO-TO (longitudinal-optical, transverse-optical) curves split at the Γ point.[31] Oxygen and chlorine have isotropic Born effective charges with values of $-1.795\,e$ and $-1.283\,e$, respectively. The diagonal Born effective charges of Na are $Z_{xx} = 0.938\,e$ and $Z_{yy} = Z_{zz} = 1.070\,e$. The calculated Born effective charges of O, Cl, and the average one of Na are quite the same as their nominal ionic charges $-2e$, $-e$, and $+e$, which is the characteristic of a pure ionic crystal. For cubic crystal, their electronic and ionic dielectric tensors are diagonal and have only one independent component.[32] The dielectric tensor of Na_3OCl has identical diagonal values of about 3.0 which is larger than the theoretically reported result of 1.97 using TB-mBJ functional.[33] Up to now, no experimental report on the dielectric constant of this material is reported. The instability at M and R points, indicating the motion of sodium in these modes, leads to a rotation of octahedra Na_6O.[14] The unstable modes imply that the crystal energy can be lowered through octahedral tilts generating the other 14 tilt structures. In Fig. 1(b), the partial density of states indicates that the unstable modes are concerned only with the Na ions. Most of the lower frequency stable modes are distributed by Cl. O and Na reign the high-frequency modes above approximately 5 THz.

The soft modes at M and R points are expressed by M_3^+ and R_4^+ irreducible representations, where M_3^+ is in-phase tilting and R_4^+ is out-of-phase tilting.[34] Figure 2(a) shows the top view of the cubic nontilted crystal structure. The M_3^+ distortion results in an in-phase rotation, as shown in Fig. 2(b), and it corresponds to the $a^0a^0c^+$ structure following the Glazer's notation.[16] Similarly, the R_4^+ distortion results in an out-of-phase rotation, as presented in Fig. 2(c), and it corresponds to $a^0a^0c^-$. The structure of the monoclinic $P2_1/m$ Na_3OCl results from the $M_3^+ \oplus R_4^+$ distortions as shown in Fig. 2(d). The tilt is in-phase along the a axis and the tilts along the b and c axes are out-of-phase, which gives the Glazer's notation of $a^+b^-c^-$. The negative frequency at M point leads to M_3^+ distortion that derives to 4 tilted systems $a^0a^0c^+$, $a^0b^+b^+$, $a^+a^+a^+$, and $a^+b^+c^+$. The irreducible representations R_4^+ led from soft mode at R point are related to 6 tilted systems $a^0a^0c^-$, $a^0b^-b^-$, $a^-a^-a^-$, $a^0b^-c^-$, $a^-b^-b^-$, and $a^-b^-c^-$. The $M_3^+ \oplus R_4^+$ distortions result in 4 tilted systems $a^0b^+c^-$, $a^+b^-b^-$, $a^+b^-c^-$, and $a^+a^+c^-$.[34] As a whole, M_3^+ and R_4^+ distortions of space group $Pm\bar{3}m$ can generate 14 tilt systems.

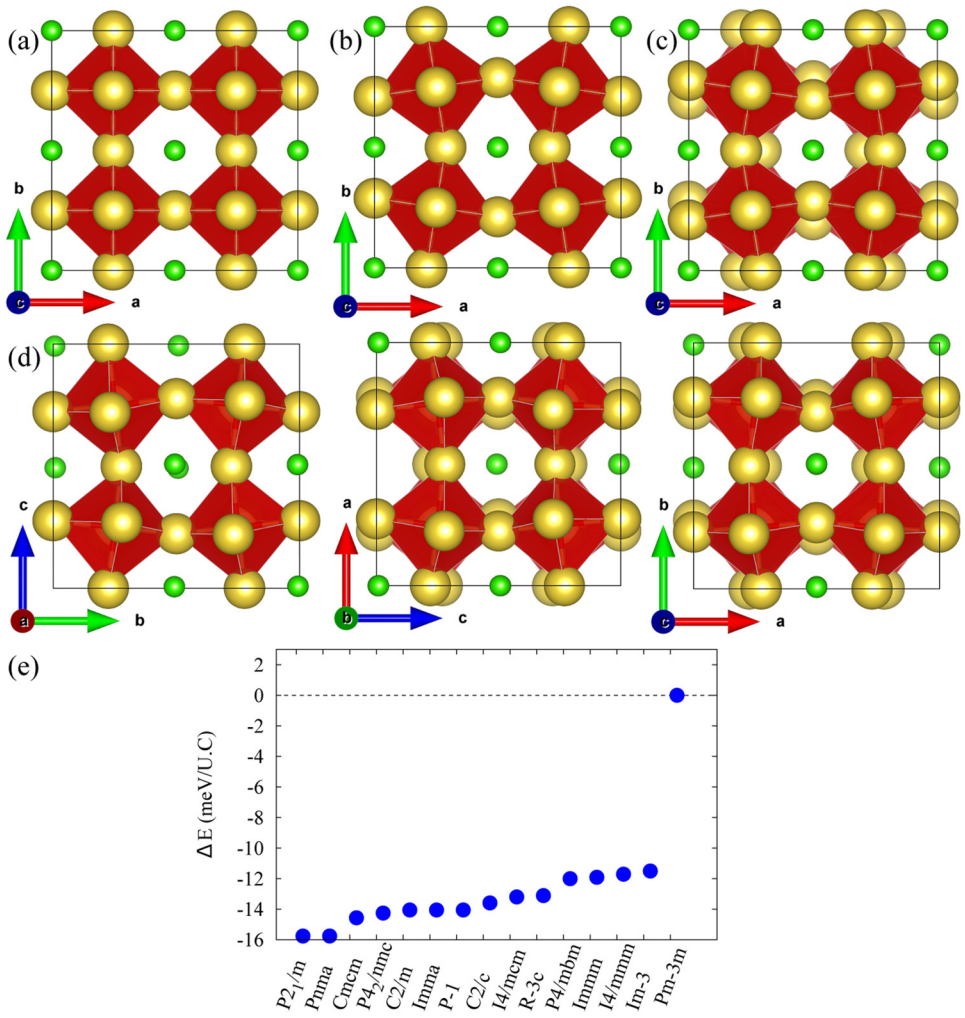

FIG. 2. (a) Nontilted cubic $Pm\bar{3}m$ crystal structure is denoted by $a^0a^0a^0$. (b) M_3^+ distortion indicates in-phase rotation (the same rotation direction of octahedral layers along an axis) which is simply presented by $a^0a^0c^+$ structure. (c) The tilted $a^0a^0c^-$ system indicates R_4^+ distortion carried by out-of-phase rotation (the alternating rotation of octahedral layers along an axis). (d) Three different views of the tilted $a^+b^-c^-$ (monoclinic $P2_1/m$) structure resulting from the combination $M_3^+ \oplus R_4^+$ distortions. (e) Energy profile of the 14 tilted structures relative to the nontilted cubic $Pm\bar{3}m$ Na_3OCl. For comparison, the energies of tilted structures are transformed into the energies per $1\times1\times1$ unit cell. All the 14 tilted structures of Na_3OCl are lower in energy than the cubic $Pm\bar{3}m$ nontilted structure where monoclinic $P2_1/m$ is the most stable structure.

TABLE I. The tilt angles θ_x, θ_y, θ_z, lattice parameters a, b, c, and α, β, γ in the 14 tilt systems of Na_3OCl.

Tilt systems	$a^0a^0c^+$	$a^0a^0c^-$	$a^0b^-b^-$	$a^0b^+b^+$	$a^0b^-c^-$	$a^0b^+c^-$	$a^-a^-a^-$
Space group	P4/mbm	I4/mcm	Imma	I4/mmm	C2/m	Cmcm	R$\bar{3}$c
θ_x (°)	8.753	8.889	8.972	8.459	8.930	9.270	7.324
θ_y (°)	8.753	8.889	6.798	6.230	6.243	6.628	7.324
θ_z (°)	0.000	0.000	6.798	6.230	7.206	7.033	7.324
a (Å)	9.0315	9.0311	9.0435	9.0358	9.0764	9.0352	9.0657
b (Å)	9.0315	9.0311	9.0759	9.0803	9.0764	9.0783	9.0657
c (Å)	9.1256	9.1268	9.0759	9.0803	9.0764	9.0739	9.0657
α (°)	90	90	89.840	90	89.827	90	89.794
β (°)	90	90	90	90	90	90	90.206
γ (°)	90	90	90	90	90	90	89.794
Tilt systems	$a^+a^+a^+$	$a^+a^+c^-$	$a^-b^-b^-$	$a^+b^-b^-$	$a^-b^-c^-$	$a^+b^-c^-$	$a^+b^+c^+$
Space group	Im$\bar{3}$	P4$_2$/nmc	C2/c	Pnma	P$\bar{1}$	P2$_1$/m	Immm
θ_x (°)	7.006	8.042	4.354	7.830	6.202	7.890	2.691
θ_y (°)	7.006	8.197	8.646	8.254	7.289	8.228	8.420
θ_z (°)	7.006	6.413	8.649	8.256	8.954	8.294	8.714
a (Å)	9.0666	9.0544	9.1058	9.0635	9.0839	9.0645	9.1189
b (Å)	9.0666	9.0544	9.0419	9.0604	9.0675	9.0625	9.0398
c (Å)	9.0666	9.0811	9.0419	9.0604	9.0425	9.0613	9.0320
α (°)	90	90	89.869	89.995	89.993	90.009	90
β (°)	90	90	90.099	90	90.005	90	90
γ (°)	90	90	89.900	90	89.850	90	90

The energetic stability of ionic crystals is typically reported in a variety of manners, such as the formation energy, the cohesive energy, and the lattice energy.[35] Figure 2(e) presents the calculated energies of all the 14 tilt systems relative to cubic Pm$\bar{3}$m Na_3OCl ($\Delta E = E_{tilt} - E_{nontilt}$, where E_{tilt} is the energy of a tilt system and $E_{nontilt}$ is the energy of cubic Pm$\bar{3}$m Na_3OCl). The energies are calculated using a $2 \times 2 \times 2$ unit cell (U.C.) and an $8 \times 8 \times 8$ k-point mesh for each structure. Space groups of 15 systems agree well with the previous study of tilting octahedra in perovskites.[17] For Li_3OCl, 10 tilted structures are more stable than the cubic phase and the remaining 4 structures are energetically close to the cubic phase. The maximum energy difference between the cubic phase and the most stable structure of Li_3OCl is less than 1 meV/U.C.[15] While all the 14 tilted structures of Na_3OCl are much lower in energy than the cubic Pm$\bar{3}$m nontilted structure with the energy differences ranging from 11 to 16 meV/U.C., the energetically most stable structure is P2$_1$/m. By using the exchange-correlation functional with LDA, the computed energy of monoclinic P2$_1$/m relative to cubic Pm$\bar{3}$m is −27 meV/U.C., and the most stable structure is unchanged. The cohesive energy of Na_3OCl is defined as $E_{coh} = [(3E_{Na} + E_O + E_{Cl}) - E_{Na_3OCl}]$, where E_{Na}, E_O, and E_{Cl} refer to the total energies of isolated Na, O, and Cl atoms, respectively. The cohesive energy of the nontilted Na_3OCl in Pm$\bar{3}$m phase is 15.560 eV/U.C. The formation energy (E_f) of Na_3OCl is defined as $E_f = \left[E_{Na_3OCl} - (3E_{Na(bcc)} + \frac{1}{2}E_{O_2} +\right.$

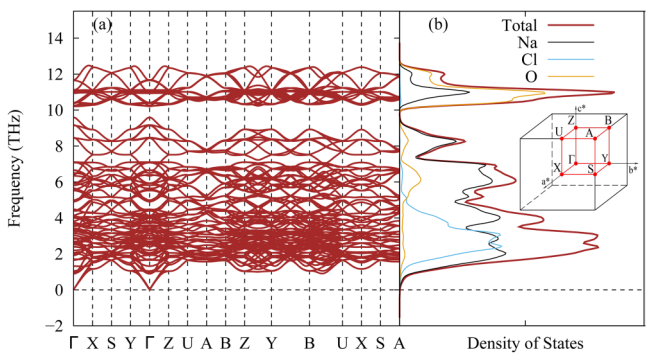

FIG. 3. (a) Phonon dispersion curves and (b) total and partial densities of states of monoclinic P2$_1$/m. The phonon dispersion curves and the total density of states show no negative modes, which proves the monoclinic P2$_1$/m is dynamically stable.

TABLE II. The relative atomic positions of the tilted structure in monoclinic P2$_1$/m (space group 11).

Atom type	Wyckoff position	Atomic coordinates
Na	4(f)	(0.47556, 0.25003, 0.52664)
		(0.52444, 0.24997, 0.97336)
		(0.47512, 0.47338, 0.24996)
		(0.52488, 1.02662, 0.25004)
	2(e)	(1/4, 0.52857, 0.51930)
		(1/4, 0.48113, 0.97095)
		(1/4, 0.98113, 0.47095)
		(1/4, 1.02857, 1.01930)
O	2(d)	(0, 1/2, 1/2)
	2(c)	(0, 1/2, 0)
	2(b)	(0, 0, 1/2)
	2(a)	(0, 0, 0)
Cl	2(e)	(1/4, 0.24368, 0.25831)
		(1/4, 0.24164, 0.75628)
		(1/4, 0.74164, 0.25628)
		(1/4, 0.74368, 0.75831)

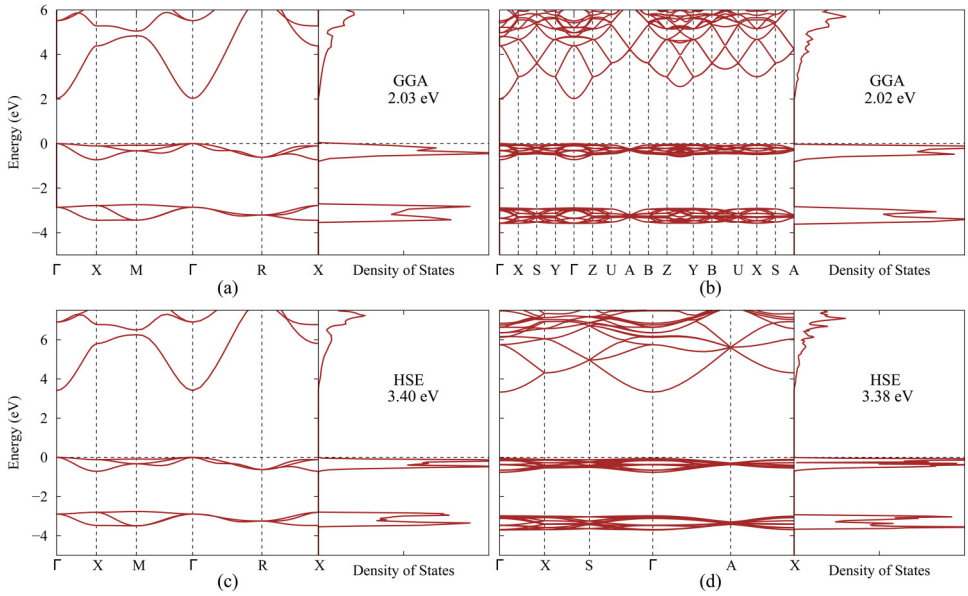

FIG. 4. Electronic band structures and density of states of [(a), (c)] cubic $Pm\bar{3}m$ and [(b), (d)] monoclinic $P2_1/m$ using the GGA and HSE methods.

$\frac{1}{2}E_{Cl_2}$)], where E_{Na_3OCl}, $E_{Na(bcc)}$, E_{O_2}, and E_{Cl_2} refer to the total energies of bulk Na_3OCl, bulk Na in body-centered-cubic (bcc) phase, and gas phase O_2 and Cl_2 molecules, respectively. The formation energy of Na_3OCl per primitive cell is equal to −7.932 eV.

The tolerance factor of an antiperovskite A_3XY is defined as $t = \frac{r_Y + r_A}{\sqrt{2}(r_X + r_A)}$, where r_X, r_Y, and r_A are the radii of the X-anion, Y-anion, and A-cation, respectively. The tolerance factor of Na_3OCl is 0.83, which increases to 0.87 for Na_3OBr and 0.94 for Na_3OI. The ionic radii of a Na cation and Cl, Br, I, and O anions are taken from Shannon's data.[36] It suggests that the substitution of Cl with larger ions results in increasing tolerance factor and it approaches 1. In other words, the cubic phase becomes favorable in case of larger substituents for Cl where the Na_6O octahedral tilt will lead to higher energy.[32,37] However, consistent with energy and phonon calculations, the lower tolerance factor (0.83) suggests that the cubic phase is not favorable for Na_3OCl and the Na_6O tilt is needed to achieve the stable phase.

The tilt angles of 14 structures are shown in Table I. The tilt angles θ_x, θ_y, and θ_z are defined by the displacements of Na atoms after rotation with respect to nontilted position of Na atoms. θ_x, θ_y, and θ_z are tilt angles along [100], [010], and [001] directions, respectively. The tilt angles range from 2.6° to 9.3°. For Li_3OCl, the tilt angles are reported to have the values ranging from 1° to 2° in P4/mbm and I4/mcm structures.[15] Since the ionic radius of Na is larger than that of Li, Na_3OCl has a little lower tolerance factor than Li_3OCl. As expected, we observed larger tilt angles in Na_3OCl than that for Li_3OCl.

After this, we have calculated the lattice vibrations of all 14 tilted structures to find out the most stable structure. In Fig. 3, no negative frequency in phonon dispersion curves is shown for monoclinic $P2_1/m$, which confirms its dynamic stability. Therefore, $P2_1/m$ is both energetically and vibrationally stable while the other 13 tilt systems have unstable phonon curves as well as higher energies. The total and partial phonon densities of states in Fig. 3(b) strongly determine the stability of monoclinic $P2_1/m$ since the calculation takes place on a dense k mesh that fully describes the first Brillouin zone. The chosen k-paths in the first Brillouin zone of monoclinic $P2_1/m$ are presented in Fig. 3(b) as well. The relative atomic positions of Na_3OCl are shown in Table II in terms of Wyckoff positions in the monoclinic $P2_1/m$.

Since the band gap of the nontilted Na_3OCl (2.03 eV) is underestimated with the GGA calculation, we also report its HSE results in Fig. 4(c) where the band gap increases to 3.40 eV. Figure 4(b) implies that the tilted Na_3OCl in monoclinic $P2_1/m$ has the direct band gap of 2.02 eV at the Γ point from the GGA calculation while the band gap increases to 3.38 eV using the HSE method. From this result, we found that the band gap is not much affected by the octahedral tilt for these two phases. To the best of our knowledge, there are no reports on the electronic structure of the tilted and nontilted Na_3OCl to compare with our results.

The static dielectric tensor of monoclinic $P2_1/m$ is nearly diagonal with the value of 2.91. Because of the low symmetry of monoclinic $P2_1/m$, the Born effective charge tensor is not completely diagonal, but the off-diagonal components are negligible and the three diagonal elements are close to each other. The average Born effective charges of Na, Cl, and O are 1.01 e, −1.25 e, and −1.784 e, respectively, in monoclinic $P2_1/m$ structure. The average Bader charges of Na, Cl, and O are 0.823 e, −0.927 e, and −1.542 e, respectively. Since the calculated Born effective charges and Bader charges of Na, Cl, and O are similar to their nominal ionic charge $+e$, $-e$, and $-2e$, respectively, we can consider monoclinic $P2_1/m$ as an ionic crystal.

IV. CONCLUSION

With the density functional theory calculations, we studied the energetics of antiperovskite Na_3OCl with titled Na_6O octahedra. By using the group-theoretical analysis of octahedral tilting in perovskites by Howard and Stokes, we examined the stability of 14 tilted structures of Na_3OCl. The 14 tilted structures of Na_3OCl were energetically more stable than the cubic $Pm\bar{3}m$ structure, and the $P2_1/m$ phase is

energetically the most stable one. Similar to literature, we found unstable phonon modes at the M and R points for the cubic $Pm\bar{3}m$ phase of Na_3OCl. These unstable modes disappeared for the $P2_1/m$ phase of the Na_3OCl. Thus, we conclude that the $P2_1/m$ phase is energetically and dynamically the most stable phase of antiperovskite Na_3OCl. In addition, we find that the cubic $Pm\bar{3}m$ phase has a direct band gap of 3.4 eV at the Γ point, and the monoclinic $P2_1/m$ phase has a quite similar result (3.38 eV), which indicates that the material is insulating. The Born effective charge and Bader charge calculations of Na, Cl, and O atoms are similar to their nominal ionic charge which confirms the ionic characteristic of cubic $Pm\bar{3}m$ and monoclinic $P2_1/m$ of antiperovskite Na_3OCl.

SUPPLEMENTARY MATERIAL

See supplementary material for X-ray diffraction spectra of the cubic $Pm\bar{3}m$ and monoclinic $P2_1/m$.

ACKNOWLEDGMENTS

This research was supported by the research grant from University of Ulsan (No. 2016-0082).

[1]T. He, Q. Huang, A. P. Ramirez, Y. Wang, K. A. Regan, N. Rogado, M. A. Hayward, M. K. Haas, J. S. Slusky, K. Inumara, H. W. Zandbergen, N. P. Ong, and R. J. Cava, Nature **411**, 54 (2001).
[2]Y. Sun, C. Wang, L. Chu, Y. Wen, M. Nie, and F. Liu, Scr. Mater. **62**, 686 (2010).
[3]P. Tong and Y. P. Sun, Adv. Cond. Matter Phys. **2012**, 903239 (2012).
[4]A. Emly, E. Kioupakis, and A. Van der Ven, Chem. Mater. **25**, 4663 (2013).
[5]M. Bilal, S. Jalali-Asadabadi, R. Ahmad, and I. Ahmad, J. Chem. **2015**, e495131 (2015).
[6]D. Matsunami, A. Fujita, K. Takenaka, and M. Kano, Nat. Mater. **14**, 73 (2014).
[7]Y. Zhao and L. L. Daemen, J. Am. Chem. Soc. **134**, 15042 (2012).
[8]M. H. Braga, J. A. Ferreira, V. Stockhausen, J. E. Oliveira, and A. El-Azab, J. Mater. Chem. A **2**, 5470 (2014).
[9]H. Nguyen, S. Hy, E. Wu, Z. Deng, M. Samiee, T. Yersak, J. Luo, S. P. Ong, and Y. S. Meng, J. Electrochem. Soc. **163**, A2165 (2016).
[10]M. H. Braga, N. S. Grundish, A. J. Murchison, and J. B. Goodenough, Energy Environ. Sci. **10**, 331 (2017).
[11]K. Hippler, S. Sitta, P. Vogt, and H. Sabrowsky, Acta Crystallogr. C **46**, 736 (1990).
[12]Y. Zhao and L. L. Daemen, J. Am. Chem. Soc. **134**, 15042 (2012).
[13]Y. Zhang, Y. Zhao, and C. Chen, Phys. Rev. B **87**, 134303 (2013).
[14]V. I. Zinenko and N. G. Zamkova, Ferroelectrics **265**, 23 (2002).
[15]M.-H. Chen, A. Emly, and A. Van der Ven, Phys. Rev. B **91**, 214306 (2015).
[16]A. M. Glazer, Acta Crystallogr. B **28**, 3384 (1972).
[17]C. J. Howard and H. T. Stokes, Acta Crystallogr. B **54**, 782 (1998).
[18]A. Samad, M. Noor-A-Alam and Y.-H. Shin, J. Mater. Chem. A **4**, 14316 (2016).
[19]A. Samad, A. Shafique, and Y.-H. Shin, Nanotechnology **28**, 175401 (2017).
[20]A. Samad, A. Shafique, H. J. Kim, and Y.-H. Shin, J. Mater. Chem. A **5**, 11094 (2017).
[21]A. Samad and Y.-H. Shin, ACS Appl. Mater. Interfaces **9**, 29942 (2017).
[22]G. Kresse and J. Furthmüller, Phys. Rev. B **54**, 11169 (1996).
[23]J. P. Perdew, K. Burke, and M. Ernzerhof, Phys. Rev. Lett. **77**, 3865 (1996).
[24]G. Kresse and D. Joubert, Phys. Rev. B **59**, 1758 (1999).
[25]A. Togo and I. Tanaka, Scr. Mater. **108**, 1 (2015).
[26]A. Kokalj, J. Mol. Graph. Model. **17**, 176 (1999).
[27]V. K. Aliaksandr, A. V. Oleg, F. I. Artur, and E. S. Gustavo, J. Chem. Phys. **125**, 224106 (2006).
[28]C. Y. Fong, J. E. Pask, and L. H. Yang, *Half-metallic Materials and Their Properties* (World Scientific, 2013). p. 304.
[29]J. C. Grossman, L. Mitas, and K. Raghavachari, Phys. Rev. Lett. **75**, 3870 (1995).
[30]S. Baroni, S. de Gironcoli, A. D. Corso, and P. Giannozzi, Rev. Mod. Phys. **73**, 515 (2001).
[31]Y. Wang, S. Shang, Z.-K. Liu, and L.-Q. Chen, Phys. Rev. B **85**, 224303 (2012).
[32]Z.-L. Lv, H.-L. Cui, H. Wang, X.-H. Li, and G.-F. Ji, Phys. Status Solidi B **254**, 1700089 (2017).
[33]J. Ramanna, N. Yedukondalu, K. Ramesh Babu, and G. Vaitheeswaran, Solid State Sci. **20**, 120 (2013).
[34]M. A. Carpenter and C. J. Howard, Acta Crystallogr. B **65**, 134 (2009).
[35]B. Li, A. Michaelides, and M. Scheffler, Phys. Rev. B **76**, 075401 (2007).
[36]R. D. Shannon, Acta Crystallogr. A **32**, 751 (1976).
[37]M. Johnsson and P. Lemmens, *Handbook of Magnetism and Advanced Magnetic Materials* (American Cancer Society, 2007).